The physical origin of optical flares following GRB 110205A and the nature of the outflow *

Wei-Hong Gao

Department of Physics and Institute of Theoretical Physics, Nanjing Normal University, Nanjing 210008, China; *gaoweihong@njnu.edu.cn*

Abstract The optical emission of GRB 110205A is distinguished by two flares. We examine two possible scenarios for the optical afterglow emission. In the first scenario, the first optical flare is the reverse shock emission of the main outflow and the second one is powered by the prolonged activity of the central engine. However, we find that it is rather hard to reasonably interpret the late ($t > 0.1$ d) afterglow data unless the GRB efficiency is very high (~ 0.95). In the second scenario, the first optical flare is the low energy prompt emission and the second one is the reverse shock of the initial outflow. Within this scenario we can interpret the late afterglow emission self-consistently. The reverse shock region may be weakly magnetized and the decline of the second optical flare may be dominated by the high latitude emission, for which strong polarization evolution accompanying the quick decline is possible, as suggested by Fan et al. in 2008. Time-resolved polarimetry by RINGO2-like polarimeters will directly test our prediction.

Key words: gamma rays: bursts — polarization — GRBs: jets and outflows — radiation mechanisms: non-thermal

1 INTRODUCTION

GRB 110205A was triggered and located by the *Swift* Burst Alert Telescope (BAT) at 02:02:41 UT and the BAT lightcurve showed activity with multiple peaks ending at 1500 s after the GRB trigger, with a peak count rate of 4500 count s^{-1} (15–150 keV) at 210 s after the trigger. The duration of GRB 110205A was $T_{90} = 257 \pm 25$ s in the range from 15 keV to 350 keV (Beardmore et al. 2011; Markwardt et al. 2011).

The redshift of GRB 110205A was $z = 2.2$ through detecting and analyzing the optical spectrum of the host galaxy (Cenko et al. 2011). As observed by Konus-Wind, the isotropic energy was $E_{\mathrm{iso}} = (4.34 \pm 0.42) \times 10^{53}$ erg, using a standard cosmology model with $H_0 = 71$ km s^{-1} Mpc^{-1}, $\Omega_{\mathrm{M}} = 0.27$ and $\Omega_{\Lambda} = 0.73$ (Gorosabel et al. 2011).

The optical observation started at 90.6 s after the GRB 110205A trigger (Klotz et al. 2011b). Two optical flares were detected during the observation. The optical brightness increased to the first peak of $R \sim 16.7$ about 225 s after the trigger. Then the flux decreased to $R \sim 18$ about 360 s after the trigger (Klotz et al. 2011a). The brightness increased again, and the second peak was $R \sim 13.7$ at
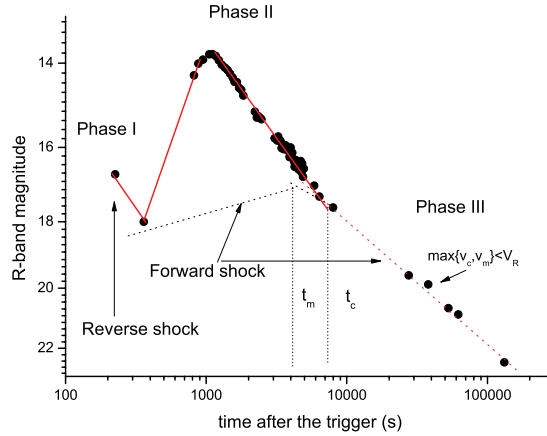
Fig. 1 Interpretation of the optical emission of GRB 110205A: the first scenario. The data points are taken from Klotz et al. (2011a,b), Andreev et al. (2011) and Kelemen (2011).

about 1140 s after the trigger (Andreev et al. 2011). The lightcurve of the optical flares in the R-band is illuminated in Figure 1. By fitting a power law $F_t \propto t^{-\alpha}$ to this lightcurve, we find $\alpha_{\mathrm{I}} \sim 2.5$ for the decline of the first flare, and $\alpha_{\mathrm{IIr}} \sim -4$ for the rising phase of the second flare. For the second flare's decline, we can obtain $\alpha_{\mathrm{IId}} \sim 2.4$ until a break at $t \sim 8000\,\mathrm{s}$, when it decayed as $F_t \propto t^{-1.6}$.

The XRT began observing GRB 110205A at 02:05:16.8 UT, 155.4 s after the BAT trigger (Beardmore et al. 2011). The X-ray lightcurve is comprised of a number of flares followed by a power-law decay. The late-time lightcurve can be modeled with a power-law decay with an index of $\alpha_{\mathrm{x}} = 1.63 \pm 0.10$ from the time 5.1×10^3 s after the trigger (Beardmore 2011).

Obviously, after the break at $t \sim 8000$ s, the optical decay should be the forward shock emission of the afterglow, with the same decay slope as that of the X-ray afterglow.

In this work we focus on the physical origin of the optical afterglow emission and pay special attention to the magnetization of the emitting region. The possible high linear polarization of the second flare will be discussed in some detail.

2 THE PHYSICAL ORIGIN OF THE OPTICAL EMISSION OF GRB 110205A

The optical lightcurve of GRB 110205A is distinguished by two flares. To interpret the data we divide the observed R-band lightcurve into three segments: phase-I is the decline phase of the first flare, phase II is the the second flare up to $t \sim 8000$ s (i.e., the break time in the decline) and phase III is the late afterglow (see Fig. 1).

In this section, we focus on two possible scenarios. In the first scenario, phase-I is the reverse shock emission of the main outflow, and phase-II is the optical flare powered by the prolonged activity of the central engine. In the second scenario, phase-I is the low energy tail of the prompt soft γ-ray emission, and phase-II is the reverse shock emission of the initial outflow. In both scenarios, phase-III is the regular forward shock afterglow emission.

2.1 The First Scenario

The early optical emission may be powered by the reverse shock. The time when the reverse shock crosses the GRB shell can be estimated as $t_\times \sim \max[T_{90}, t_{\rm dec}]$, where $t_{\rm dec}$ is the deceleration time of the fireball and is given by

$$t_{\rm dec} = [(3E_{\rm k}/4\pi\gamma_0^2 nm_{\rm p}c^2)^{1/3}/2\gamma_0^2 c](1+z),$$

where γ_0 is the initial Lorentz factor of the GRB outflow, n is the number density of the circum-burst medium, c is the speed of light, $m_{\rm p}$ is the rest mass of protons, and $E_{\rm k}$ is the isotropic-equivalent kinetic energy of the GRB outflow. Here we assume $E_{\rm k} = 5E_{\rm iso}$, corresponding to a moderate GRB efficiency $\eta_\gamma \equiv E_{\rm iso}/(E_{\rm iso} + E_{\rm k}) \approx 0.17$. The thick shell case corresponds to $T_{90} \sim t_\times$ while the thin shell case corresponds to $T_{90} < t_\times$.

For the current burst, the reverse shock emission peaks at $t_{\rm p,r} = 225$ s, where superscript "r" represents the parameter of the reverse shock, hence we have

$$t_\times \sim t_{\rm p,r} \sim T_{90} \sim t_{\rm dec}$$

and

$$\gamma_0 \sim \left[\frac{24E_{\rm k}(1+z)^3}{\pi nm_{\rm p}c^5 t_{\rm p,r}^3}\right]^{1/8} = 4.3 \times 10^2 E_{\rm k,54.3}^{1/8} n_0^{-1/8} t_{\rm p,r,2.4}^{-3/8}\left(\frac{1+z}{3.2}\right)^{3/8}.$$

When reverse shock crosses the thick shell, its emission is governed by (Sari & Piran 1999 and Kobayashi 2000)

$$\nu_{\rm m}^{\rm r}(t_\times) \approx 5.0 \times 10^{13} \epsilon_{\rm e,-1}^{\rm r}{}^2 \epsilon_{\rm B,-2}^{\rm r}{}^{1/2} n_0^{1/2} \gamma_{0,2.6}^2 \left(\frac{1+z}{3.2}\right)^{-1} \text{Hz}, \tag{1}$$

$$\nu_{\rm c}^{\rm r}(t_\times) \approx 8.5 \times 10^{14} \epsilon_{\rm B,-2}^{\rm r}{}^{-3/2} E_{\rm k,54.3}^{-1/2} n_0^{-1}\left(\frac{1+z}{3.2}\right)^{-1/2} t_{\times,2.4}^{-1/2} \text{Hz}, \tag{2}$$

$$F_{\nu,\max}^{\rm r}(t_\times) \approx 5.1 \times 10^2 \epsilon_{\rm B,-2}^{\rm r}{}^{1/2} E_{\rm k,54.3}^{5/4} n_0^{1/4} \gamma_{0,2.6}^{-1} t_{\times,2.4}^{-3/4}\left(\frac{1+z}{3.2}\right) D_{\rm L,28.7}^{-2} \text{mJy}, \tag{3}$$

where $\epsilon_{\rm B}$ and $\epsilon_{\rm e}$ are the fractions of the shock energy given to the magnetic field and electrons at the shock front respectively and $D_{\rm L}$ is the luminosity distance. The synchrotron emission for $\nu_{\rm m}^{\rm r} < \nu_{\rm R} < \nu_{\rm c}^{\rm r}$ is estimated by

$$F_{\nu_{\rm R}}^{\rm r} = F_{\nu,\max}^{\rm r}(\nu_{\rm R}/\nu_{\rm m}^{\rm r})^{-(p-1)/2} \approx 50\epsilon_{\rm B,-2}^{\rm r}\epsilon_{\rm e,-1}^{\rm r}{}^2 E_{\rm k,54.3}^{5/4} n_0^{3/4} \gamma_{0,2.6} t_{\times,2.4}^{-3/4} D_{\rm L,28.7}^{-2} \text{mJy},$$

where p is the power-law index of the electron distribution (i.e., $N_\gamma \propto \gamma^{-p}$). For $t > t_\times$, the reverse shock emission drops with time as $F_\nu^{\rm r} \propto t^{-(73p+21)/96}$ (Kobayashi 2000; Fan et al. 2002). Taking $p = 3$, we can get $F_\nu^{\rm r} \propto t^{-2.5}$, matching the decline of the first flare. The reverse shock's optical emission flux can be consistent with the observation for proper parameters, such as $\epsilon_{\rm e}^{\rm r} \sim 0.1$, $\epsilon_{\rm B,-2}^{\rm r} \sim 0.1$ and $n_0 \sim 10^{-2}$.

It is however important to check whether the late ($t > 0.1$ d) afterglow emission can be interpreted as the forward shock emission. For $t > 0.1$ d, the X-ray and optical afterglow data decline with the time as $t^{-1.6}$, suggesting that the R-band is above both the typical synchrotron radiation frequency ($\nu_{\rm m}$) and the cooling frequency ($\nu_{\rm c}$) of the forward shock electrons. Therefore both ν_c and ν_m should cross the observer's frequency ($\nu_{\rm R}$) before $t < 0.1$ d. These two times are denoted as $t_{\rm c}$ and $t_{\rm m}$, respectively.

For the ISM-like medium[1] and $t > t_{\text{dec}}$, we have $F_{\nu,\text{max}} \propto t^0$, $\nu_m \propto t^{-3/2}$ and $\nu_c \propto t^{-1/2}$ (Sari & Piran 1999). In the fast cooling case, the forward shock emission can be estimated as

$$F_\nu = \begin{cases} (\nu/\nu_c)^{1/3} F_{\nu,\text{max}} \propto t^{1/6}, & \nu_m > \nu_c > \nu, \\ (\nu/\nu_c)^{-1/2} F_{\nu,\text{max}} \propto t^{-1/4}, & \nu_m > \nu > \nu_c, \\ (\nu_m/\nu_c)^{-1/2}(\nu/\nu_m)^{-p/2} F_{\nu,\text{max}} \propto t^{-3/2}, & \nu > \nu_m > \nu_c, \end{cases} \tag{4}$$

where $p \sim 2.6$ has been adopted[2]. Evidently, the forward shock R-band emission should be dimmer than 18th mag at $t = 350\,\text{s}$ and then be the same as that detected at $t > 0.1\,\text{d}$. It is straightforward to show that it is not possible to find t_c and t_m with the scaling laws of Equation (4). Hence this possibility has been ruled out.

In the slow cooling case,

$$F_\nu = \begin{cases} (\nu/\nu_m)^{1/3} F_{\nu,\text{max}} \propto t^{1/2}, & \nu_c > \nu_m > \nu, \\ (\nu/\nu_m)^{-(p-1)/2} F_{\nu,\text{max}} \propto t^{-6/5}, & \nu_c > \nu > \nu_m, \\ (\nu_c/\nu_m)^{-(p-1)/2} (\nu/\nu_c)^{-p/2} F_{\nu,\text{max}} \propto t^{-3/2}, & \nu > \nu_c > \nu_m. \end{cases} \tag{5}$$

In this case one can find proper $t_c \sim 4 \times 10^3\,\text{s}$ and $t_m \sim 8 \times 10^3\,\text{s}$, as illustrated in Figure 1. Hence it deserves a further investigation. For $t > t_{\text{dec}}$, the dynamics of the forward shock can be well approximated by an approach similar to the Blandford-McKee solution (Blandford & McKee 1976), from which emission can be estimated by

$$F_{\nu,\text{max}} = 23\,\text{mJy} \left(\frac{1+z}{3.2}\right) D_{\text{L},28.7}^{-2} \epsilon_{\text{B},-2}^{1/2} E_{\text{k},54.3} n_0^{1/2}, \tag{6}$$

$$\nu_m = 9.0 \times 10^{15}\,\text{Hz}\, E_{\text{k},54.3}^{1/2} \epsilon_{\text{B},-2}^{1/2} \epsilon_{e,-1}^2 \left(\frac{C_{\text{p}}}{1.6}\right)^2 \left(\frac{1+z}{3.2}\right)^{1/2} t_3^{-3/2}, \tag{7}$$

$$\nu_c = 2.3 \times 10^{15}\,\text{Hz}\, E_{\text{k},54.3}^{-1/2} \epsilon_{\text{B},-2}^{-3/2} n_0^{-1} \left(\frac{1+z}{3.2}\right)^{-1/2} t_3^{-1/2}, \tag{8}$$

where

$$C_p \equiv 13(p-2)/[3(p-1)].$$

As shown in Figure 1, the data suggest that $F_{\nu,\text{max}} \sim 0.4\,\text{mJy}$, i.e.,

$$\epsilon_{\text{B},-2}^{1/2} E_{\text{k},54.3} n_0^{1/2} \sim 1/60.$$

The fact that ν_m and ν_c cross ν_{R} at t_m and t_c gives that

$$E_{\text{k},54.3}^{1/2} \epsilon_{\text{B},-2}^{1/2} \epsilon_{e,-1}^2 \sim 0.5$$

and

$$E_{\text{k},54.3}^{-1/2} \epsilon_{\text{B},-2}^{-3/2} n_0^{-1} \sim 0.6.$$

To reproduce the data, one needs $\epsilon_{\text{B},-2} \sim 4 \times 10^7 E_{\text{k},54.3}^3$, which is hard to satisfy for reasonable GRB efficiency. Let us check whether the inverse Compton effect can change the result or not. With such an effect, $\nu_c \propto (1+Y)^{-2}$, where Y is the Compton parameter and can be estimated by

$$Y \sim (-1 + \sqrt{1 + 4\eta\epsilon_e/\epsilon_{\text{B}}})/2,$$

---

[1] In the case of the free stellar-wind medium, the decline of the forward shock emission after the peak of the reverse shock cannot be shallower than $t^{-1/4}$ (e.g., see table 1 of Xue et al. 2009). On the other hand, the forward shock R-band emission should be dimmer than 18th mag at $t = 350\,\text{s}$ and then be the same as that detected at $t \geq 0.1\,\text{d}$. With Figure 1 it is straightforward to show that such conditions cannot be satisfied. So we do not discuss the wind medium model here.

[2] Such a value is roughly consistent with that needed to account for the late afterglow decline ($F \propto t^{-1.6}$) and that required to reproduce the late time X-ray spectrum ($F_\nu \propto \nu^{-1.15\pm0.08}$).

where

$$\eta \sim \min\left\{1, \left[\frac{\nu_{\mathrm{m}}}{(1+Y)^2\nu_{\mathrm{c}}}\right]^{(p-2)/2}\right\}.$$

For $t \sim t_{\mathrm{c}} \sim t_{\mathrm{m}}$, we have $\nu_{\mathrm{c}} \sim \nu_{\mathrm{m}}$, $\quad \eta \sim (1+Y)^{2-p}$ and $Y \sim (\epsilon_{\mathrm{e}}/\epsilon_{\mathrm{B}})^{0.4}$, if $\eta\epsilon_{\mathrm{e}}/\epsilon_{\mathrm{B}} \gg 1$. So the cooling frequency is estimated by

$$\nu_{\mathrm{c}} = 3.6 \times 10^{14}\,\mathrm{Hz}\, E_{\mathrm{k},54.3}^{-1/2}\epsilon_{\mathrm{e},-1}^{-0.8}\epsilon_{\mathrm{B},-2}^{-0.7}n_0^{-1}\left(\frac{1+z}{3.2}\right)^{-1/2}t_3^{-1/2}$$

(for $t_{\mathrm{c}} \sim 8 \times 10^3$ s, we have $E_{\mathrm{k},54.3}^{-1/2}\epsilon_{\mathrm{e},-1}^{-0.8}\epsilon_{\mathrm{B},-2}^{-0.7}n_0^{-1} \sim 4$). In this case we need $\epsilon_{\mathrm{B}} \sim 6 \times 10^{-9}E_{\mathrm{k},54.3}^{-3.4}$ to reproduce the data, which seems too small to be reasonable. A reasonable $\epsilon_{\mathrm{B}} \sim 10^{-3} - 10^{-2}$ is obtainable if we take $E_{\mathrm{k}} \sim E_{\mathrm{iso}}/20$, i.e., the GRB efficiency is as high as $\eta_\gamma \sim 0.95$. It is unclear how such a high GRB efficiency can be achieved. Indeed, very high η_γ have been reported for some Swift GRBs in the literature (e.g., Zhang et al. 2007; Cenko et al. 2010). One, however, should view these preliminary results with caution. For example, in the energy injection model for the shallow X-ray decline phase, a very high η_γ can be obtained if one estimates E_{k} with the shallow decline data. However, as pointed out by Fan & Piran (2006) for the first time, in many cases the energy injection model cannot be used to interpret the simultaneous optical data self-consistently. Therefore the very high GRB efficiency found in the specific energy injection model is questionable. For some bursts, for instance GRB 080319B, the prompt gamma-ray emission plausibly came from a narrow energetic core while the late time afterglow emission was powered by wider but much less powerful ejecta (e.g., Racusin et al. 2008). The derived GRB efficiency would be unreasonably high if one estimates E_{k} with the late afterglow data rather than the early afterglow data. Considering these uncertainties, we do not examine the ultra-high η_γ model further.

Since neither the slow nor the fast cooling case can provide a self-consistent interpretation of the forward shock emission, we conclude that the first scenario is not favored.

2.2 The Second Scenario

The BAT observation showed that the prompt soft gamma-ray emission with multiple peaks lasted to > 300 s after the trigger. That means when the first optical flare peaked at about 225 s, the prompt gamma-ray emission was still ongoing. So it is possible that phase-I is the low energy tail of prompt emission. Indeed bright prompt optical emission has been well detected in some GRBs, such as GRB 041219A (Blake et al. 2005) and GRB 080319B (Racusin et al. 2008). In this case phase-II may be powered by the reverse shock of the initial prompt GRB. If correct, the fireball is thin since the reverse shock crossed the outflow at a time $t_\times \sim 1140$ s $\gg T_{90}$. The initial Lorentz factor of the GRB outflow can be estimated as

$$\gamma_0 \sim \left[\frac{24E_{\mathrm{k}}(1+z)^3}{\pi n m_{\mathrm{p}}c^5 t_\times^3}\right]^{1/8} = 2.8 \times 10^2 E_{\mathrm{k},54.3}^{1/8}n_0^{-1/8}t_{\times,3.1}^{-3/8}\left(\frac{1+z}{3.2}\right)^{3/8}. \tag{9}$$

In the thin shell case, for $\nu_{\mathrm{m}}^{\mathrm{r}} < \nu_{\mathrm{R}} < \nu_{\mathrm{c}}^{\mathrm{r}}$ and $t < t_\times$, $F_{\nu_{\mathrm{R}}}^{\mathrm{r}} \propto t^{2p-1} \propto t^{4.2}$ (e.g., Fan et al. 2002), consistent with the rising behavior of phase-II $F_{\nu_{\mathrm{R}}} \propto t^4$. The decline of phase-II is expected to show $F_{\nu_{\mathrm{R}}} \propto t^{-(27p+5)/35}$ if it is dominated by the synchrotron radiation of the cooling reverse shock electrons or alternatively $F_{\nu_{\mathrm{R}}} \propto t^{-[2+(p-1)/2]}$ if dominated by the high latitude emission of the reverse shock, in agreement with the observation for $p \sim 2.6$ (we will return to this point later). Therefore both the increase and the decline of phase-II can be reasonably interpreted within the reverse shock model.

Following Fan et al. (2002), the peak optical emission of the reverse shock can be estimated as

$$F_{\nu_{\mathrm{R}}}^{\mathrm{r}} \approx 3\,\mathrm{mJy}\,[8(p-2)/3(p-1)]^{p-1}\epsilon_{\mathrm{e},-1}^{\mathrm{r}}{}^{p-1}\epsilon_{\mathrm{B},-3}^{\mathrm{r}}{}^{(p+1)/4}n_0^{(p+1)/4}(\gamma_0/280)^{p+1}, \tag{10}$$

where the total number of the reverse-shock-accelerated electrons $\sim E_k/\gamma_0 m_p c^2$ and the strength of reverse shock $\Gamma_{rs} \sim 1.3$ have been adopted. For proper parameters, for example $\epsilon_B^r \sim \epsilon_e^r \sim 0.1$ and $n_0 \sim 1$, the reverse shock emission is so bright that it can account for the observational data.

As in the first scenario, it is important to check whether the forward shock emission can account for the late afterglow data. In principle there could be three regimes.

Case I: $\nu_R > \max\{\nu_m(t_\times), \nu_c(t_\times)\}$, for which the temporal behaviors of the forward shock optical emission are given by (e.g., Xue et al. 2009)

$$F_{\nu_R} \propto \begin{cases} t^2, & \text{for } t < t_\times, \\ t^{-1.5}, & \text{for } t > t_\times. \end{cases} \tag{11}$$

Case II: $\nu_m(t_\times) < \nu_R < \nu_c(t_\times)$. In this case, the expression

$$t_c = 2.1 \times 10^4 \, \text{s} \, E_{k,54.3}^{-1} \epsilon_{B,-2}^{-3} n_0^{-2} \left(\frac{1+z}{3.2}\right)^{-1},$$

at which time ν_c crosses the observer's frequency, should be introduced. The temporal behaviors of the forward shock optical emission are given by (e.g., Xue et al. 2009)

$$F_{\nu_R} \propto \begin{cases} t^3, & \text{for } t < t_\times, \\ t^{-1.2}, & \text{for } t_\times < t < t_c, \\ t^{-1.5}, & \text{for } t > t_c. \end{cases} \tag{12}$$

Case III: $\nu_c(t_\times) < \nu_R < \nu_m(t_\times)$. In this case, we introduce

$$t_m = 6.8 \times 10^3 \, \text{s} \, E_{k,54.3}^{1/3} \epsilon_{B,-2}^{1/3} \epsilon_{e,-1}^{4/3} \left(\frac{1+z}{3.2}\right)^{1/3},$$

when ν_m crosses the observer's frequency. The temporal behaviors of the forward shock's optical emission are given by (e.g., Xue et al. 2009)

$$F_{\nu_R} \propto \begin{cases} t^2, & \text{for } t < t_\times, \\ t^{-1/4}, & \text{for } t_\times < t < t_m, \\ t^{-1.5}, & \text{for } t > t_m. \end{cases} \tag{13}$$

This causes the forward shock optical emission to be dimmer than $\sim 18^{\text{th}}$ mag at $t \sim 350\,\text{s}$ and it should be consistent with the afterglow data for $t > 0.1\,\text{d}$. With the temporal behaviors suggested in Case-I, the predicted optical emission at $t \sim 350\,\text{s}$ is much brighter than $\sim 18^{\text{th}}$ mag, rendering this possibility unlikely.

Usually, the cooling frequency of the forward shock emission is comparable to or larger than than that of the reverse shock. In the modeling of the temporal behaviors of phase-II, the cooling frequency of the reverse shock is required to be above ν_R. Therefore Case-III is disfavored and just Case-II remains. As shown in Figure 2, Case-II works as long as $t_c \leq 8 \times 10^3\,\text{s}$.

After the reverse shock crossed the ejecta, the cooling frequency of the reverse shock's electrons drops with time as $t^{-3/2}$ (Sari & Piran 1999). Therefore, $\nu_c^r(t_\times) \geq (t_c/t_\times)^{3/2}\nu_R$ is needed if the quickly decaying optical emission is the synchrotron radiation of the cooling reverse shock electrons (hereafter the synchrotron radiation case). Alternatively $\nu_c^r(t_\times) \geq (t_c/t_\times)\nu_R$ is needed if the quickly decaying optical emission is dominated by the high latitude emission of the reverse shock (hereafter the high latitude emission case). However, we have $\nu_c(t_\times) \approx (t_c/t_\times)^{1/2}\nu_R$. Therefore, we need

$$\nu_c^r(t_\times) \sim (t_c/t_\times)\nu_c(t_\times)$$

or

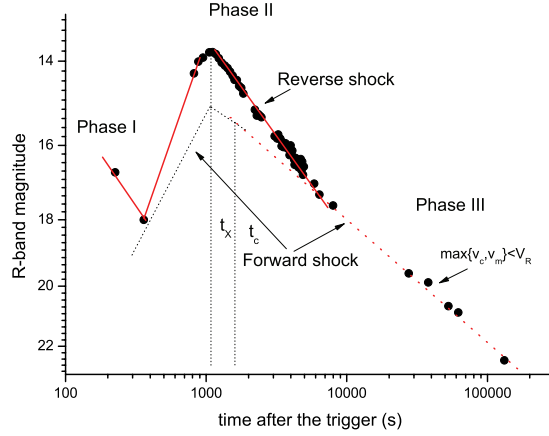$$\nu_c^r(t_\times) \sim (t_c/t_\times)^{1/2}\nu_c(t_\times).$$

Fig. 2 Interpretation of the optical emission of GRB 110205A: the second scenario.

Following Jin & Fan (2007), we have

$$\nu_c^r(t_\times) \sim \Re_B^{-3}\left(\frac{1+Y}{1+Y^r}\right)^2 \nu_c(t_\times),$$

where $Y^r > 0$ is the Compton parameter of the reverse shock. Note that

$$\nu_m^r \sim 3 \times 10^{11}\,\mathrm{Hz}\ \epsilon_{e,-1}^{r}{}^2 \epsilon_{B,-2}^{r}{}^{1/2} n_0^{1/2} \ll \nu_c^r$$

unless $\epsilon_{e,-1}^r \equiv \Re_e \epsilon_{e,-1} \sim 10$ (Fan et al. 2002), therefore $Y^r \leq 1$ for $(\nu_m^r/\nu_c^r)^{(2-p)/2}(\epsilon_e^r/\epsilon_B^r) \leq 1$. Hence we have $\nu_c^r(t_\times) \sim \Re_B^{-3}(1+Y)^2\nu_c(t_\times)$, which further gives $\Re_B \sim 0.5(1+Y)^{2/3}$ (synchrotron radiation case) or $\Re_B \sim 0.7(1+Y)^{2/3}$ (high latitude emission case), implying the outflow could be (weakly) magnetized for $Y \sim (\epsilon_e/\epsilon_B)^{0.4} \geq 1$.

A magnetized outflow is also consistent with the flux analysis. In Case-II, the ratio between the reverse shock optical emission and forward shock optical emission at the crossing time of the reverse shock can be estimated by (Jin & Fan 2007; Fan et al. 2002; Zhang et al. 2003)

$$\frac{F_{\nu_R}^r(t_\times)}{F_{\nu_R}(t_\times)} \approx 0.08\Re_e^{p-1}\Re_B^{\frac{p+1}{2}} = 0.08\Re_e^{1.6}\Re_B^{1.8}. \tag{14}$$

The current observation suggests that

$$F_{\nu_R}^r(t_\times)/F_{\nu_R}(t_\times) \geq 4,$$

so we then have

$$\Re_e^{1.6}\Re_B^{1.8} \geq 50,$$

i.e.,

$$\Re_B \geq 8.8\Re_e^{-0.9}. \tag{15}$$

For $\Re_e \leq 10$ we have $\Re_B \geq 1$ unless phase-II was dominated by the emission of prolonged activity of the central engine (e.g., Gao 2009).

3 THE EXPECTED POLARIZATION PROPERTY OF THE OPTICAL FLARES

The polarimetry of prompt emission or the reverse shock emission is very important for diagnosing the composition of the GRB outflow. Since the late afterglow, taking place hours after the trigger, is powered by the external forward shock, essentially all the initial information about the ejecta is subsequently lost. If the GRB ejecta is initially magnetized, the prompt γ-ray/X-ray/UV/optical emission and the reverse shock emission should be linearly polarized (Lyutikov et al. 2003; Granot 2003; Fan et al. 2004). In a few events, the prompt γ-ray polarimetry is available but the results are quite uncertain. Even for the very bright GRB 041219A, a systematic effect that could mimic the weak polarization signal could not be excluded (McGlynn et al. 2007). So far, the most reliable polarimetry is that in the UV/optical band (e.g., Covino et al. 1999). The optical polarimetry of the prompt emission or the reverse shock emission demands a quick response of the telescope to the GRB alert and is thus very challenging. Nevertheless, significant progress has been made since 2006. Using a ring polarimeter on the robotic Liverpool Telescope, Mundell et al. (2007) got an upper limit of $\sim 8\%$ for the optical polarization of the afterglow of GRB 060418 at 203 s after the trigger. A breakthrough was made in GRB 090102, for which Steele et al. (2009) found out that the reverse shock emission was linearly polarized with a degree of $\sim 10.1\%$. The forward-reverse shock modeling of the afterglow emission suggests a mildly magnetized reverse shock region (Fan 2009; Mimica et al. 2010). These two findings are consistent with each other and provide the most compelling evidence so far for the magnetized outflow model for GRBs.

For the current event, we have shown that phase-I may be the low energy tail of the prompt emission and phase-II is likely the reverse shock emission, though another possibility, the prolonged activity of the central engine, cannot be ruled out. In the reverse shock model we find out that the initial outflow could be weakly magnetized. Assuming that in the emitting region the strength ratio of the ordered magnetic field and the random magnetic field is b, the degree of net polarization can be roughly estimated as $\Pi_{\mathrm{net}} \approx 0.6b^2/(1+b^2)$ (e.g., Fan et al. 2004). Therefore a moderate or high linear-polarization-degree of the weakly magnetized reverse shock emission is possible. In reality, the configuration of the outflowing magnetic field may be very complicated and the direction of the lines may not be well ordered, so the net polarization degree should be lowered. In Section 2.2 we have shown that the decline of the second optical flare may be dominated by the high latitude emission of the reverse shock. In such a case, an interesting polarization degree evolution is present if at late times (i.e., $t > t_\times$) the edge of the ejecta is visible (see fig. 2 of Fan et al. 2008 for illustration). Alternatively, if the decline of the second optical flare is shaped by the synchrotron radiation of the cooling reverse shock electrons, the observed linear polarization should be

$$\Pi = (\Pi^{\mathrm{r}} F_{\nu_{\mathrm{R}}}^{\mathrm{r}} + \Pi F_{\nu_{\mathrm{R}}})/(F_{\nu_{\mathrm{R}}}^{\mathrm{r}} + F_{\nu_{\mathrm{R}}}),$$

where $\Pi \sim 1.4\%$ (Π^{r}) is the linear polarization of the forward (reverse) shock emission (Gorosabel et al. 2011) and $F_{\nu_{\mathrm{R}}}$ ($F_{\nu_{\mathrm{R}}}^{\mathrm{r}}$) is the R-band flux of the forward (reverse) shock emission. One thus expects a steady decline of the polarization degree with time.

The Liverpool Telescope began automatically observing Swift GRB 110205A with the RINGO2 polarimeter (Mundell et al. 2011). RINGO2 is quite sensitive and can measure the linear polarization degree down to 0.9% for a source as bright as $R = 17$ mag with an exposure time of 100 s. Therefore, the linear polarization of the first optical flare might be detectable if it is significantly polarized. For the second optical flare, the emission is so bright that the time-resolved polarization property can be achieved. The observations of the Liverpool Telescope on GRB 110205A have stopped due to bad weather and the polarization data have not yet been published. Nevertheless, the current optical data have shed some light on the nature of the GRB outflow and have suggested very interesting polarization properties.

4 CONCLUSIONS AND DISCUSSION

The early optical emission of GRB 110205A is characterized by two flares. Two possible scenarios have been examined in this work. In the first scenario, the first optical flare is the reverse shock emission of the main outflow, the second flare is the emission powered by the prolonged activity of the central engine, and the late time ($t > 0.1$ d) optical emission is the regular forward shock emission. However we find that a self-consistent interpretation of the forward shock emission is hard to achieve unless the GRB efficiency is ~ 0.95. Therefore this scenario is disfavored. In the second scenario, the first optical flare is the low energy prompt emission while the second flare is the reverse shock emission of the main outflow. The late optical emission is still attributed to the regular forward shock. Within this scenario a self-consistent interpretation is achieved (please note that the different inverse Compton parameters for the reverse and forward shocks play an important role in the modeling). There are two interesting findings. One is that the reverse shock region may be weakly magnetized and a moderate linear polarization degree is likely. The other is that the decline of the second optical flare may be dominated by the high latitude emission. Similar to the X-ray case, one may expect a dramatic polarization evolution (Fan et al. 2008) accompanying the optical flare decline rather than the steady decrease in polarization degree. In reality the configuration of the out-flowing magnetic field may be very complicated and the direction of the lines may not be well ordered, for which the net polarization degree should be lowered and the polarization evolution may be very complicated.

The Liverpool Telescope began automatically observing Swift GRB 110205A with the RINGO2 polarimeter (Mundell et al. 2011). RINGO2 is very sensitive. The linear polarization of the first optical flare may be detectable if it is significantly polarized. For the second optical flare, the emission is so bright that time-resolved polarization properties can be achieved. Therefore our prediction, in particular strong polarization evolution in the decline phase of the second optical flare, can be directly tested.

References

Andreev, M., Sergeev, A., & Pozanenko, A. 2011, GRB Coordinates Network, Circular Service, 11641, 1

Beardmore, A. P. 2011, GRB Coordinates Network, Circular Service, 11644, 1

Beardmore, A. P., Baumgartner, W. H., Burrows, D. N., et al. 2011, GRB Coordinates Network, Circular Service, 11629, 1

Blake, C. H., Bloom, J. S., Starr, D. L., et al. 2005, Nature, 435, 181

Blandford, R. D., & McKee, C. F. 1976, Physics of Fluids, 19, 1130

Cenko, S. B., Frail, D. A., Harrison, F. A., et al. 2010, ApJ, 711, 641

Cenko, S. B., Hora, J. L., & Bloom, J. S. 2011, GRB Coordinates Network, Circular Service, 11638, 1

Covino, S., Lazzati, D., Ghisellini, G., et al. 1999, A&A, 348, L1

Fan, Y., & Piran, T. 2006, MNRAS, 369, 197

Fan, Y.-Z. 2009, MNRAS, 397, 1539

Fan, Y.-Z., Dai, Z.-G., Huang, Y.-F., & Lu, T. 2002, ChJAA (Chin. J. Astron. Astrophys.), 2, 449

Fan, Y. Z., Wei, D. M., & Wang, C. F. 2004, A&A, 424, 477

Fan, Y.-Z., Xu, D., & Wei, D.-M. 2008, MNRAS, 387, 92

Gao, W.-H. 2009, ApJ, 697, 1044

Gorosabel, J., Duffard, R., Kubanek, P., & Guijarro, A. 2011, GRB Coordinates Network, Circular Service, 11696, 1

Granot, J. 2003, ApJ, 596, L17

Jin, Z. P., & Fan, Y. Z. 2007, MNRAS, 378, 1043

Kelemen, J. 2011, GRB Coordinates Network, Circular Service, 11726, 1

Klotz, A., Gendre, B., Lass, M., Boer, M., & Atteia, J. L. 2011a, GRB Coordinates Network, Circular Service, 11632, 1

Klotz, A., Gendre, B., Lass, M., Boer, M., & Atteia, J. L. 2011b, GRB Coordinates Network, Circular Service, 11630, 1

Kobayashi, S. 2000, ApJ, 545, 807

Lyutikov, M., Pariev, V. I., & Blandford, R. D. 2003, ApJ, 597, 998

Markwardt, C. B., Barthelmy, S. D., Baumgartner, W. H., et al. 2011, GRB Coordinates Network, Circular Service, 11646, 1

McGlynn, S., Clark, D. J., Dean, A. J., et al. 2007, A&A, 466, 895

Mimica, P., Giannios, D., & Aloy, M. A. 2010, MNRAS, 407, 2501

Mundell, C. G., Smith, R. J., & Cano, Z. 2011, GRB Coordinates Network, Circular Service, 11633, 1

Mundell, C. G., Steele, I. A., Smith, R. J., et al. 2007, Science, 315, 1822

Racusin, J. L., Karpov, S. V., Sokolowski, M., et al. 2008, Nature, 455, 183

Sari, R., & Piran, T. 1999, ApJ, 520, 641

Steele, I. A., Mundell, C. G., Smith, R. J., Kobayashi, S., & Guidorzi, C. 2009, Nature, 462, 767

Xue, R.-R., Fan, Y.-Z., & Wei, D.-M. 2009, A&A, 498, 671

Zhang, B., Kobayashi, S., & Mészáros, P. 2003, ApJ, 595, 950

Zhang, B., Liang, E., Page, K. L., et al. 2007, ApJ, 655, 989